Langmuir

Article

pubs.acs.org/Langmuir

Drug-Loaded Fluorescent Cubosomes: Versatile Nanoparticles for Potential Theranostic Applications

Sergio Murgia,*[,†] Sara Bonacchi,[‡] Angela M. Falchi,[§] Sandrina Lampis,[†] Vito Lippolis,[†] Valeria Meli,[†] Maura Monduzzi,[†] Luca Prodi,[‡] Judith Schmidt,[#] Yeshayahu Talmon,[#] and Claudia Caltagirone*[,†]

[†]Dipartimento di Scienze Chimiche e Geologiche, Università di Cagliari, s.s. 554 bivio Sestu, I-09042 Monserrato (CA), Italy

[‡]Dipartimento di Chimica "G. Ciamician", Università degli Studi di Bologna, via Selmi 2, 40126 Bologna, Italy

[§]Dipartimento di Scienze Biomediche, Università di Cagliari, s.s. 554 bivio Sestu, I-09042 Monserrato (CA), Italy

[#]Department of Chemical Engineering, Technion - Israel Institute of Technology, Haifa 32000, Israel

Supporting Information

ABSTRACT: In this work, monoolein-based cubosomes were doped with two fluorescent probes, namely, fluorescein and dansyl, properly modified with a hydrocarbon chain to increase their encapsulation efficiency within the monoolein palisade. The same nanocarriers were also loaded with quercetin, a hydrophobic molecule with potential anticancer activity. Particularly, the cubosomes doped with the modified fluorescein probe were successfully exploited for single living cell imaging. The physicochemical and photophysical characterizations reported here, along with the well-known ability of cubosomes in hosting molecules with pharmaceutical interest, strongly encourage the use of these innovative fluorescent nanocarriers for theranostic purposes.

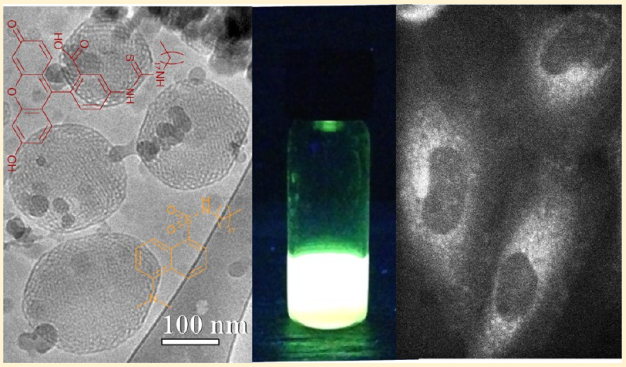

INTRODUCTION

Application of nanotechnology to medicine (nanomedicine) holds promise to deeply reform the diagnostic and therapeutic tools available in clinical practice.[1,2] Indeed, nanotechnology offers a unique possibility to improve both imaging and drug delivery techniques. To reach this goal, a myriad of nanocarriers, belonging to soft and hard matter, have been engineered and tested for their physicochemical, pharmaceutical, and cytotoxic features. Relevant examples include liposome formulations,[3−6] polymeric,[7−11] gold, or iron oxide nanoparticles, as well as dendrimers and quantum dots.[12] Nanoparticles were originally developed to transport separately pharmaceutically active or imaging agents to the pathological sites with therapeutic or diagnostic scopes. Recently, both of these aspects were merged into single platforms, thus forming theranostic nanomedicine, an emerging cross-discipline, where chemistry, biology, pharmacy, and medicine meet.[13] Therefore, within the same dosage, theranostic nanoparticles may (actively or passively) deliver both drugs and imaging probes to the site of disease, overcoming the differences in biodistribution and selectivity of these two distinct entities and reducing side effects.[14−20] Although many kinds of nanoparticles have been proposed for theranostic applications,[21−26] cubosomes have until now been neglected. Cubosomes are lipid-based nanoparticles sterically stabilized by pluronics[27−30] that can be envisaged as aqueous dispersions of bicontinuous cubic liquid-crystalline phases. Briefly, they are constituted of curved, triply periodic non-intersecting bilayers folded on an infinite periodic minimal surface having cubic symmetry and organized to form two disjointed continuous water channels.[31] Cubosomes, which can be regarded as the nonlamellar analogue of liposomes, show high mechanical rigidity and structural stability and may be loaded with both hydrophobic and hydrophilic drugs (including proteins),[32] taking advantage also of their huge interfacial surface area per unit of volume. Indeed, with respect to liposomes, cubosomes possess a greater hydrophobic volume that, in principle, allows encapsulating higher amounts of poor water-soluble drugs. Moreover, they are mostly prepared using monoolein, a monolgyceride that can be easily biodegraded by lipases.[33,34] Due to these features, cubosomes are often suggested as drug delivery systems useful in parenteral administration (i.e., all routes of drug administration different from mouth).[32] However, they possess further appealing features that could be exploited in theranostic nanomedicine. Indeed, they are sufficiently large to avoid a rapid clearance from the bloodstream while their nanostructure is enclosed within a PEG corona that, similarly to stealth liposomes, should protect cubosomes against opsonisation (opsonins are proteins that bind to foreign particles, allowing phagocytic cell recognition) and consequent clearance from the bloodstream.[12]

Received: March 22, 2013
Revised: May 3, 2013
Published: May 6, 2013

With the aim of exploring the potentiality of aqueous cubosome dispersions for theranostic applications, in this work, we decorated cubosomes with two modified fluorophores and loaded this kind of nanoparticle with a therapeutic dose of quercetin (3,3′,4′,5,7-pentahydroxyflavone). Two commercially available fluorophores, namely, fluorescein and dansyl, were functionalized with a C18 hydrocarbon chain to give, respectively, F1 and F2 (Figure 1). Particularly, quercetin is a

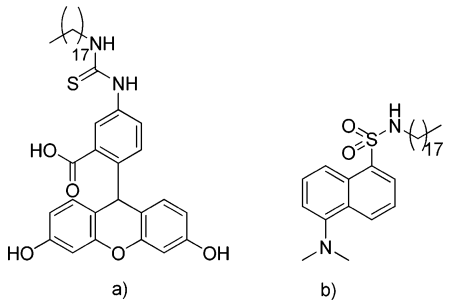

Figure 1. Fluorophores F1 (a) and F2 (b).

polyphenolic compound widely distributed in plants that, similarly to many other hydrophobic drugs, has a limited clinical use due to its poor water solubility with a consequent very low bioavailability. Quercetin exerts multiple pharmacological effects. Among these, a potent in vivo antioxidant activity, induction of apoptosis, modulation of cell cycle, antimutagenesis, inhibition of angiogenesis, and anti-inflammatory effects are well-recognized. Moreover, quercetin is considered to be an anticancer drug since some studies have shown its inhibitory effects on tumor growth.[35−37]

MATERIALS AND METHODS

Chemicals. Monoolein (MO, 1-monooleoylglycerol, RYLO MG 19 PHARMA, glycerol monooleate; 98.1 wt %) was kindly provided by Danisco A/S, DK-7200, Grinsted, Denmark. Pluronic F108 (PEO_{132}−PPO_{50}−PEO_{132}), quercetin, fluorescein isothiocyanate isomer I (90%), dansyl chloride (≥95%), octadecylamine (≥99%), sodium sulfate (≥99.0%), potassium carbonate (99%), acetonitrile (≥99.9%), diethyl ether (≥99.5%), dichloromethane (≥99%), and tetrahydrofuran (≥99%) were purchased from Sigma-Aldrich. Distilled water passed through a Milli-Q water purification system (Millipore) was used to prepare the samples.

Sample Preparation. Cubic phases were prepared by weighing the appropriate amounts of components (MO, water, quercetin, and fluorophore) into glass tubes ($L \approx 0.5$ cm) that were immediately sealed, centrifuged at 2300 rpm at 25 °C, and allowed to equilibrate at 25 °C for 1 week. Cubosomes, empty or doped with the fluorophore molecule, were prepared by dispersing the appropriate amount of MO in a solution of Pluronic F108 using an ultrasonic processor UP100H by Dr. Hielscher, cycle 0.9, amplitude 90%, for 10 min. To obtain fluorescent cubosomes, the fluorophore was dispersed in the melted monoolein with the help of an ultrasonic bath before dispersion in Pluronic F108. The sample volume was usually 4 mL with approximately 96.4 wt % of water, 3.3 wt % of MO, and 0.3 wt % of Pluronic F108. The percentage of the fluorophore was 2.5×10^{-3} and 2.8×10^{-3} wt % for F1 and F2, respectively. The same procedure was followed when the fluorescent cubosomes were also loaded with quercetin. The percentage of added quercetin was 6.4×10^{-6} wt %.

Light Microscopy. The homogeneous liquid-crystalline phases were observed by optical microscopy (Zeiss Axioplan II) in polarized light at 25 °C.

Cryogenic Transmission Electron Microscopy (Cryo-TEM). Vitrified specimens were prepared in a controlled environment vitrification system (CEVS) at 25 °C and 100% relative humidity. A drop of the sample was placed on a perforated carbon film-coated copper grid, blotted with filter paper, and plunged into liquid ethane at its freezing point. The vitrified specimens were transferred to a 626 Gatan cryo-holder and observed at 120 kV acceleration voltage in an FEI Tecnai T12 G2 transmission electron microscope at about −175 °C in the low-dose imaging mode to minimize electron-beam radiation damage. Images were digitally recorded with a Gatan US1000 high-resolution CCD camera.

Ultrafiltration and Dialysis. Ultrafiltrated cubosomes were carried out by means of Amicon Ultra 0.5 mL centrifugal filters (RC 100 kDa, 7000 rpm/10 min). After quercetin was loaded, cubosome dispersion was purified from the non-encapsulated drug by dialysis as follows: 2 mL was loaded into a Spectra/Por membrane (12−14 kDa MW cutoff; Spectrum Laboratories Inc., USA) and dialyzed against water (1000 mL) for 2 h (by replacing the water after 1 h) at 5 °C. Drug loading efficiency (E%), expressed as percentage of the drug amount initially used, was determined by UV−vis spectroscopy after disruption of cubosomes with methanol. Quercetin content was quantified at 373 nm using a Thermo Nicolet Evolution 300 UV−vis spectrophotometer.

Dynamic Light Scattering (DLS). Particle size and ζ-potential determinations of the nanoparticles were performed with a ZetaSizer Nano ZS (Malvern Instruments, Malvern, UK) at a temperature of 25 ± 0.1 °C. Samples were backscattered by a 4 mW He−Ne laser (operating at a wavelength of 633 nm) at an angle of 173°. Diluted samples (1:50) were housed in disposable polystyrene cuvettes of 1 cm optical path length with water as solvent. At least two independent samples were taken, each of which was measured from three to five times. The width of DLS hydrodynamic diameter distribution is indicated by PDI (polydispersion index).

Photophysical Measurements. Cubosome solutions were diluted with Milli-Q water and ultrafiltered before performing the photophysical measurements. The emission and excitation spectra were recorded with an Edinburgh FLS920 equipped photomultiplier Hamamatsu R928P. The same instrument connected to a PCS900 PC card was used for the TCSPC (time-correlated single photon counting) experiments (excitation laser λ = 405 nm). Fluorescence intensities were corrected for inner filter effects according to standard methods.[38] All fluorescence anisotropy measurements were performed on an Edinburgh FLS920 equipped with Glan-Thompson polarizers. Anisotropy measurements were collected using an L-format configuration, and all data were corrected for polarization bias using the G-factor. Low-volume quartz cuvettes with an optical path length of 1.0 × 0.2 cm were used to reduce the scattering effects from the cubosome solutions.

Small-Angle X-ray Scattering (SAXS) Experiments. Small-angle X-ray scattering was recorded with a S3-MICRO SWAXS camera system (HECUS X-ray Systems, Graz, Austria). Cu Kα radiation of wavelength 1.542 Å was provided by a GeniX X-ray generator, operating at 50 kV and 1 mA. A 1D-PSD-50 M system (HECUS X-ray Systems, Graz, Austria) containing 1024 channels of width 54.0 μm was used for detection of scattered X-rays in the small-angle region. The working q range (Å^{-1}) was $0.003 \leq q \leq 0.6$, where $q = 4\pi\sin(\theta)\lambda^{-1}$ is the scattering wave vector. A stainless steel sample holder with thin polymeric sheet (Bratfolie, Kalle) windows enclosing a few milligrams of the sample was used for cubic phases, while thin-walled 2 mm glass capillaries were used for cubosome dispersions. The diffraction patterns for cubic phases and cubosomes were recorded, respectively, for 30 min and 7 h. The lattice parameter a of the cubic phases was determined using the relation $a = d(h_2 + k_2 + l_2)^{1/2}$ from linear fits of the plots of $1/d$ versus $(h_2 + k_2 + l_2)^{1/2}$, where $d = 2\pi/q$ (q is the measured peak position) and h, k, and l are the Miller indices. Water channel radii were calculated using the relation $R_w = [(A_0/-2\pi\chi)^{1/2}a] - L$, where L is the lipid length value (17 Å), a is the lattice parameter obtained from the SAXS analysis, and A_0 and χ are the surface area and the Euler characteristic of the IPMS geometries ($Ia3d$, $A_0 = 3.091$, $\chi = -8$; $Pn3m$, $A_0 = 1.919$, $\chi = -2$). To minimize scattering from air, the camera volume was kept under vacuum during the measurements. Silver behenate (CH_3−$(CH_2)_{20}$−COOAg) with a d

dx.doi.org/10.1021/la401047a | Langmuir 2013, 29, 6673−6679

Table 1. Photophysical Properties of F1 and F2 in the Bulk, Loaded Inside the Cubosomes (Aqueous Solution, pH 7 after Ultrafiltration), in Basic Aqueous Solution (F1), and in Ethanol Solution (F2)

		epsilon (M^{-1} cm^{-1})	exc[a] ($\lambda_{max/nm}$)	em[b] ($\lambda_{max/nm}$)	r[c]	τ[d] (ns)
F1	bulk cubic phase		485	544	0.2	3.9
	cubosomes (aqueous dispersion)		484	517	0.3	3.8
	H_2O buffered pH 9	89000 (λ = 500 nm)	494	517	0.0	3.0
F2	bulk cubic phase		333	500	0.1	12.7
	cubosomes (aqueous dispersion)		336	520	0.1	12.8
	EtOH	4200 (λ = 340 nm)	333	507	0.0	13.3

[a]Excitation spectra (F1, λ_{em} = 520 nm; F2, λ_{em} = 510 nm). [b]Emission spectra (F1, λ_{exc} = 470 nm; F2, λ_{exc} = 340 nm). [c]Emission anisotropy (F1, λ_{exc} = 470 nm; F2, λ_{exc} = 340 nm). [d]Average lifetime (F1 and F2, laser source λ_{exc} = 405 nm).

spacing value of 58.38 Å was used as a standard to calibrate the angular scale of the measured intensity.

Cell Cultures and Treatment. Mouse 3T3 fibroblasts (ATCC collection) were grown at 37 °C in phenol red-free Dulbecco's modified Eagle's medium (DMEM, Invitrogen, USA) with high glucose, supplemented with 10% (v/v) fetal bovine serum, penicillin (100 U mL^{-1}), and streptomycin (100 μg mL^{-1}) (Invitrogen) in a 5% CO_2 incubator at 37 °C. Cells were grown in 35 mm dishes, and experiments were carried out 2 days after seeding when cells had reached 80−90% confluence. Nanoparticle formulations were added to the cells at a concentration of 1:1000 (2 μL of sample in 2 mL of medium) and incubated at 37 °C for 3 h. For live cell imaging, the sample suspension was replaced with fresh serum-free medium before the imaging session.

Fluorescence Microscopy. Fluorescent microscopy observations of the cells were made using a Zeiss (Axioskop) upright microscope (Zeiss, Oberkochen, Germany) equipped with a filter system of 470 ± 20 nm for excitation and 535 ± 40 nm for emission, a 40×/0.75 NA water immersion objective, and a HBO 50 W L-2 mercury lamp (Osram, Berlin, Germany). Twelve-bit-deep images were acquired with a monochrome cooled CCD camera (QICAM, Qimaging, Canada) and analyzed with Image Pro Plus software (Media Cybernetics, Silver Springs, MD). The fluorescence images of cubosomes in a diluted aqueous solution mixed with ethylene glycol (see Figure 4) were obtained with an inverted microscope (Olympus IX71) equipped with a Basler CCD color camera (SC A640-70gs) and using as excitation light the 488 nm laser emission of an Ar^+ ion laser (Melles Griot, IMA1-Multiwavelength, 43 series ion laser).

RESULTS AND DISCUSSION

Here, we explored monoolein (MO)-based cubosomes doped with two hydrophobically modified fluorophores and loaded with quercetin as nanoparticles for theranostic applications. First, the two fluorophores F1 and F2 (see Figure 1) were synthesized by refluxing octadecylamine with fluorescein isothiocyanate isomer I in THF (in the case of F1) or with dansyl chloride in MeCN in the presence of K_2CO_3 (in the case of F2), to give the desired thiourea (F1) or sulfonamide (F2) in 35.5 and 74.5% yields, respectively.

Indeed, hydrophobic derivatization is a common approach to improve encapsulation of different probes within lipid nanostructures.[38] Here, it should be noticed that fluorescein cannot be easily dispersed within cubosomes. Actually, through an optical microscope, we observed crystals of this fluorophore in bulk cubic phases even at very low concentration. Therefore, to facilitate the accommodation of the fluorophores within the MO palisade while preserving the original cubosome nanostructure, fluorescein and dansyl were functionalized with a C18 hydrophobic chain to obtain the fluorophores F1 and F2 (Figure 1). Moreover, as fluorescein and dansyl are slightly water-soluble, while F1 and F2 are highly hydrophobic, the adopted approach should allow increased encapsulation efficiency in the nanoparticles.

To evaluate the capacity of the MO bicontinuous cubic phase to host the fluorophores, F1 and F2 were initially encapsulated in a MO/W (water) = 70/30 (wt %) *Ia*3*d* (gyroid) cubic bulk phase rather than in the cubosome dispersion. The fluorophore concentration was kept below a threshold of 0.1 wt % to avoid structural alterations of the original cubic nanostructure. The MO/W = 70/30 cubic samples loaded with F1 and F2 were observed with an optical microscope under polarized light to check the absence of undissolved crystals, while their fluorescence was confirmed by exposing the cubic bulk phase to ultraviolet light. Noticeably, F1 and F2 show rather strong fluorescence in the bicontinuous bulk cubic phases, with an emission maximum at 544 and 500 nm and a high anisotropy value of 0.2 and 0.1, respectively (see Table 1). Since fluorescein undergoes deactivation by self-quenching processes,[39,40] this is additional proof that the F1 fluorophore is dispersed within the MO matrix rather than self-aggregated.

Results from this preliminary study demonstrated that the optimal fluorophore concentration in the MO/W = 70/30 *Ia*3*d* cubic bulk phase was approximately 0.05 and 0.06 wt % for F1 and F2, respectively. At this concentration, no crystals were observed and strong fluorescence was detected. The preservation of the cubic nanostructure was assessed by SAXS. The diffraction pattern showed at least five Bragg peaks with relative positions in a ratio of $\sqrt{6}:\sqrt{8}:\sqrt{14}:4:\sqrt{20}$, which are characteristic of the *Ia*3*d* space group (Figure S1 in Supporting Information). The lattice parameter and the water channel radii extracted from the SAXS diffraction patterns were found to be 131.1 ± 0.3 and 15.5 Å for F1 and 130.4 ± 0.4 and 15.3 Å for F2. These structural parameters are almost identical to those found in the absence of the fluorophores. It is worth recalling here that, upon increasing the water content, the *Ia*3*d* phase evolves toward a different bicontinuous cubic phase characterized by a *Pn*3*m* (double diamond) space group. The aqueous dispersions of MO bicontinuous cubic phases (cubosomes) should possess this type of inner nanostructure since the *Pn*3*m* phase can coexist with an excess of water.

According to a bottom-up approach, fluorescent cubosomes were prepared by dispersing a melted mixture of MO and F1 or F2 in a pluronic F108 (PF108) solution via sonication. In this study, PF108 was chosen since it demonstrated superior ability in cubosome formulation.[27] Cubosome dispersions were prepared at the composition MO/W/PF108 = 3.3/96.4/0.3 (wt %), while the amount of F1 or F2 was, respectively, 2.5×10^{-3} and 2.8×10^{-3} wt %. Cubosomes were then characterized for particle size and morphology, as well as for their inner structure and photophysical properties. The cryo-TEM image of F1-doped cubosomes is reported in Figure 2. Several nanoparticles with inner cubic structure are clearly discernible. On the basis of repeated observations, the sample under

dx.doi.org/10.1021/la401047a | Langmuir 2013, 29, 6673−6679

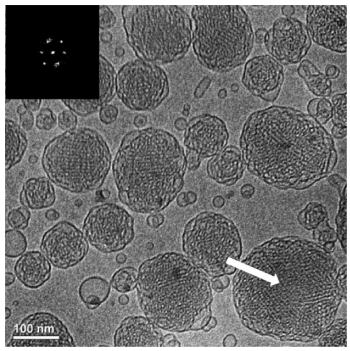

Figure 2. Cryo-TEM image of MO-based cubosomes loaded with F1. Fast Fourier transformation of the domain indicated by the arrow is shown in the inset.

investigation was found to be a dispersion of cubosomes having a diameter in the range of 100−200 nm.

The optical diffractogram obtained by the fast Fourier transform (inset in Figure 2) of the cryo-TEM image suggests the presence of an inner cubic arrangement, as it shows the typical motifs of the {111} reflection of a *Pn*3*m* phase.[41] Differently, when F2 was added to the formulation along with the expected cubosomes, a new kind of nanoparticles was observed (Figure 3). In other words, the insertion of the F2

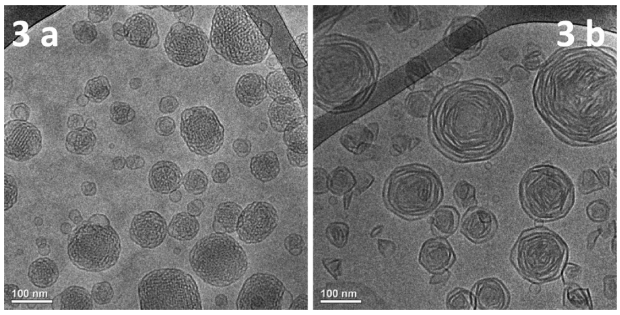

Figure 3. Cryo-TEM image of MO-based sample loaded with F2: (a) cubosomes and (b) rose-like nanoparticles.

fluorophore within the MO palisade causes a profound alteration of the surfactant packing, thus originating the new nanostructure having a rose-like morphology (Figure 3b). Such "roses" coexist with the ordered cubic phase dispersion, representing about 15% of the dispersed phase (as a rough estimate). In some cases, transition between the cubic and the rose-like morphology can be observed (see Figure S2).

The inner cubic structure of the cubosomes was confirmed by SAXS. The diffraction pattern shows at least three Bragg peaks with relative positions in a ratio of $\sqrt{2}:\sqrt{3}:2$, which are characteristics of the *Pn*3*m* phase (Figure S3). For empty or variously loaded cubosomes, Table 2 reports the structural parameters from the SAXS analysis along with mean diameters, polydispersion indexes, and ζ-potentials obtained from dynamic light scattering (DLS). Also note that, in striking agreement with cryo-TEM images, DLS analysis certifies very similar nanoparticles' dimensions, besides a quite low PDI. Concerning the F2-doped sample, given the high dilution, the characteristic pattern (if any) of the rose-like nanostructure was not discernible in the SAXS pattern.

The presence of free dye in the aqueous dispersion of cubosomes doped either with F1 or F2 was avoided by

Table 2. Lattice Parameter (a), Water Channel Radius (r_W), Mean Diameter (D_{av}), Polydispersion Index (PDI), and ζ-Potential of the Cubosome Nanoparticles Empty or Loaded with Various Cargos

cubosome cargos	a (Å)	r_W (Å)	D_{av} (nm)	PDI	ζ-potential (mV)
	98 ± 1	21.3 ± 0.8	161 ± 2	0.17	−29.4 ± 0.6
F1	101 ± 1	22.4 ± 0.8	148 ± 2	0.12	−26.6 ± 0.6
F2	98 ± 1	21.2 ± 0.8	148 ± 2	0.14	−24.5 ± 0.1
quercetin	98 ± 1	21.3 ± 0.8	161 ± 3	0.15	−25.6 ± 0.9
F1 + quercetin	99 ± 1	21.6 ± 0.8	160 ± 2	0.19	−27.6 ± 0.2
F2 + quercetin	96 ± 1	20.3 ± 0.8	159 ± 2	0.12	−22.8 ± 0.3

purifying samples via ultrafiltration. Their absence was checked through fluorescence optical microscopy observations, as exemplified in Figure 4. Particularly, to decrease the

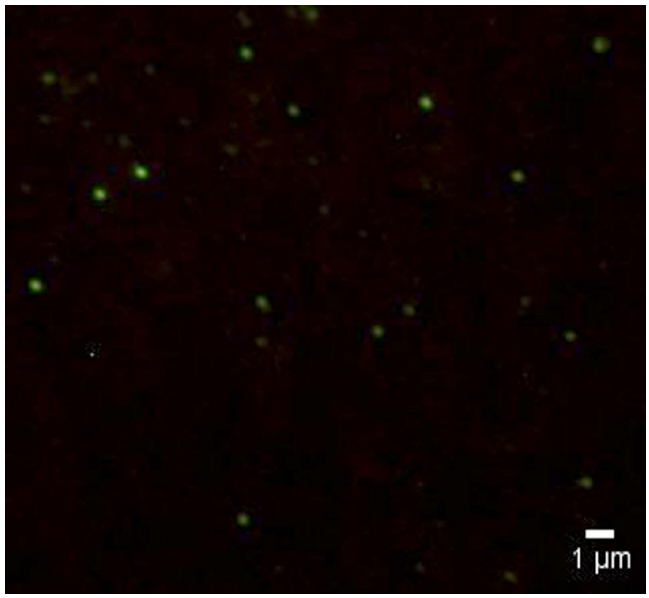

Figure 4. Fluorescence microscopy image of F1-doped cubosomes (see the text).

cubosomes' diffusion on the glass microscopy slide, the ultrafiltrated aqueous solutions of F1- and F2-doped cubosomes were diluted with ethylene glycol before the pictures were taken. If some free dye was molecularly dispersed in the aqueous phase, the image shown in Figure 4 should have appeared as a more or less homogeneous bright field. On the contrary, the fluorescent spots on a dark background observed in Figure 4 represent an additional proof that F1 is completely encapsulated within the nanoparticles. The same holds for F2.

The photophysical properties of an aqueous dispersion (pH 7) of cubosomes are very similar to those of F1 dissolved in a basic aqueous solution at pH 9 (where F1 is soluble), with a maximum of the emission band at 517 nm, an excitation band that overlaps that of F1, as shown in Figure 5, and a slightly longer averaged excited state lifetime (3.8 ns for F1 within the cubosomes and 3.0 ns for F1 in aqueous solution at pH 9; see Table 1).

These results are expected since the energetics of the $\pi-\pi^*$ excited state of the fluorescein unit is known to be independent of the polarity of the environment. A very interesting result

dx.doi.org/10.1021/la401047a | *Langmuir* 2013, 29, 6673−6679

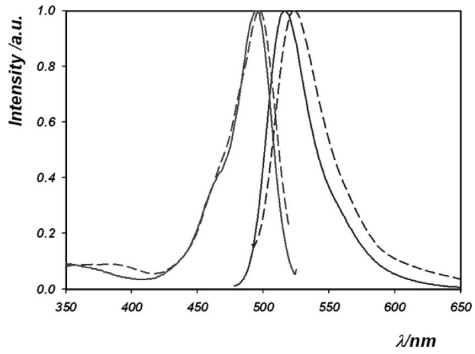

Figure 5. Normalized emission (λ_{exc} 470 nm) and excitation (λ_{em} 540 nm) spectra of MO-based cubosomes doped with F1 in an aqueous dispersion at pH 7 (dashed lines) and F1 in an aqueous dispersion buffered at pH 9 (solid line).

emerged from fluorescence anisotropy measurements. The observed value of 0.3 clearly indicates that F1 is inserted into a large structure with a reduced mobility since the anisotropy of freely mobile fluorescein is negligible. This conclusion is supported by the photophysical characterization of MO-based cubosomes doped with the dansyl derivative F2. Indeed, dansyl is known to have photophysical properties that strongly depend on the solvent polarity. We found that F2-doped cubosomes show an emission maximum at 520 nm and an excited state lifetime of 12.8 ns (see Figure S4 and Table 1).

These results are very similar to those observed for F2 in ethanol (507 nm and 13.3 ns) and very different from those reported for dansyl derivatives in water solution (560 nm and 2.9 ns in water; 500 nm and 13.4 ns in ethanol).[42] These results also confirm that F2 is embedded within the nanoparticles and give some information on its localization. Indeed, these data suggest that the fluorescent moiety of F2 is located in the same region of the MO polar heads, experiencing interactions with the MO OH groups.

On the basis of the cryo-TEM analysis, which in the case of the F2-doped cubosome dispersion evidenced the presence of nanoparticles having an inner structure different from cubic, only the cellular uptake of MO-based cubosomes doped with F1 was investigated. 3T3 fibroblast cells were incubated in the presence of nanoparticles for 3 h and imaged with fluorescent microscopy. These observations were made immediately after replacing the nanoparticle suspension in the medium with fresh particle-free medium. Diffuse fluorescence was detected in the cytosol and, particularly, in the perinuclear region of living cells (Figure 6). Therefore, as confirmed by the intracellular fluorescence detection, we can conclude that F1 penetrates into the cells via the cubosome carrier.

Finally, the F1-doped cubosome dispersion was loaded with quercetin, a polyphenolic molecule endowed of anticancer activity. The calculated loading efficiency (see the Materials and Methods section) was 80%. SAXS and DLS results reported in Table 2 demonstrate that the presence of quercetin does not significantly alter the inner nanostructure of the cubosome, as well as their size and charge. Interestingly, although pluronic-stabilized cubosomes are basically uncharged, they display a negative ζ-potential, as reported by other authors.[43,44] The origin of this negative charge is still unclear, but preferential adsorption of hydroxyl ions at the oil−water interface, as in case of oil droplets in water, has been proposed to explain the observed values of ζ-potential.[44]

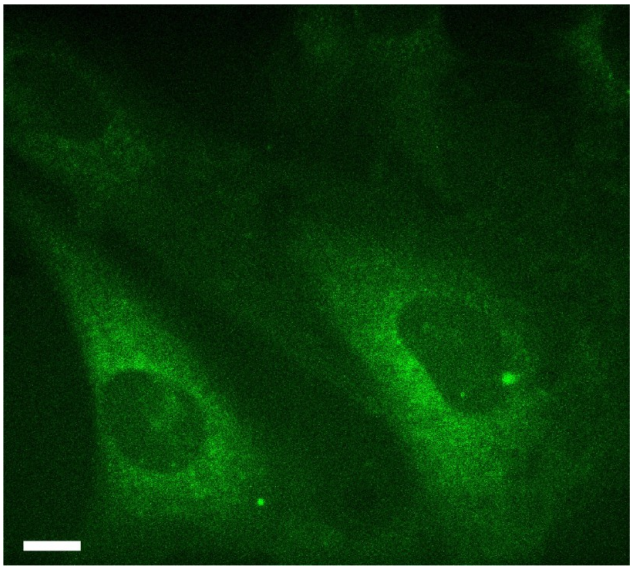

Figure 6. Fluorescence image of viable 3T3 fibroblast cells after treatment with F1-loaded MO-based cubosomes.

CONCLUSIONS

Cubosomes are often proposed as suitable drug nanocarriers,[29,32,45−47] and the ability of bicontinuous cubic phases to host molecules with pharmaceutical interest has been proved numerous times.[48,49] In this paper, we demonstrated that MO-based cubosomes, still retaining the characteristics given by their peculiar inner nanostructure, can efficiently and easily be coupled with properly designed fluorophores and loaded with an anticancer drug. Therefore, the physicochemical and photophysical measurements, along with the single living cell imaging analysis here reported, make these innovative fluorescent nanocarriers a candidate for theranostic applications.

ASSOCIATED CONTENT

Supporting Information

Additional figures as described in text. This material is available free of charge via the Internet at http://pubs.acs.org.

AUTHOR INFORMATION

Corresponding Author

*Tel: +390706754453. E-mail: murgias@unica.it (S.M.), ccaltagirone@unica.it (C.C.).

Notes

The authors declare no competing financial interest.

ACKNOWLEDGMENTS

The authors wish to thank Alessandra Garau for fruitful discussions. Financial support from MIUR is gratefully acknowledged: Projects PRIN 2009Z9ASCA and PRIN 2010BJ23MN_002. The Scientific Park "Sardegna Ricerche" is acknowledged for free access to SAXS.

REFERENCES

(1) Riehemann, K.; Schneider, S. W.; Luger, T. A.; Godin, B.; Ferrari, M.; Fuchs, H. Nanomedicine—challenge and perspectives. *Angew. Chem., Int. Ed.* **2009**, *48*, 872.

(2) Yan, Y.; Such, G. K.; Johnston, A. P. R.; Best, J. P.; Caruso, F. Engineering particles for therapeutic delivery: prospects and challenges. *ACS Nano* **2012**, *5*, 3663.

(3) Angelico, R.; Carboni, M.; Lampis, S.; Schmidt, J.; Talmon, Y.; Monduzzi, M.; Murgia, S. Physicochemical and rheological properties of a novel monoolein-based vesicle gel. *Soft Matter* **2013**, *9*, 921−928.
(4) Carboni, M.; Falchi, A. M.; Lampis, S.; Sinico, C.; Manca, M. L.; Schmidt, J.; Talmon, Y.; Murgia, S.; Monduzzi, M. Physicochemical, cytotoxic, and dermal release features of a novel cationic liposome nanocarrier. *Adv. Healthcare Mater.* **2013**, *2*, 692−701.
(5) Cuomo, F.; Ceglie, A.; Lopez, F. Specific interaction between nucleolipid doped liposomes and DNA allow a more efficient polynucleotide condensation. *J. Colloid Interface Sci.* **2012**, *365*, 184−190.
(6) Murgia, S.; Falchi, A. M.; Mano, M.; Lampis, S.; Angius, R.; Carnerup, A. M.; Schmidt, J.; Diaz, G.; Giacca, M.; Talmon, Y.; Monduzzi, M. Nanoparticles from lipid-based liquid crystals: emulsifier influence on morphology and cytotoxicity. *J. Phys. Chem. B* **2010**, *114*, 3518−3525.
(7) Angelico, R.; Ceglie, A.; Colafemmina, G.; Lopez, F.; Murgia, S.; Olsson, U.; Palazzo, G. Biocompatible lecithin organogels: structure and phase equilibria. *Langmuir* **2005**, *21*, 140−148.
(8) Hiwale, P.; Lampis, S.; Conti, G.; Caddeo, C.; Murgia, S.; Fadda, A. M.; Monduzzi, M. In vitro release of lysozyme from gelatin microspheres: effect of cross-linking agents and thermoreversible gel as suspending medium. *Biomacromolecules* **2011**, *12*, 3186−3193.
(9) Murgia, S.; Fadda, P.; Colafemmina, G.; Angelico, R.; Corrado, L.; Lazzari, P.; Monduzzi, M.; Palazzo, G. Characterization of the solutol® HS15/water phase diagram and the impact of the Δ9-tetrahydrocannabinol solubilization. *J. Colloid Interface Sci.* **2013**, *390*, 129−136.
(10) Qian, F.; Ding, J.; Tang, C.; Yin, C. Chitosan graft copolymer nanoparticles for oral protein drug delivery: preparation and characterization. *Biomacromolecules* **2006**, *7*, 2722−2727.
(11) Sivakumar, B.; Aswathy, R. G.; Nagaoka, Y.; Suzuki, M.; Fukuda, T.; Yoshida, Y.; Maekawa, T.; Sakthikumar, D. N. Multifunctional carboxymethyl cellulose-based magnetic nanovector as a theragnostic system for folate receptor targeted chemotherapy, imaging, and hyperthermia against cancer. *Langmuir* **2013**, *29*, 3453−3466.
(12) Barreto, J. A.; O'Malley, W.; Kubeil, M.; Graham, B.; Stephan, H.; Spiccia, L. Nanomaterials: applications in cancer imaging and therapy. *Adv. Mater.* **2011**, *23*, H18.
(13) Lammers, T.; Aime, S.; Hennink, W. E.; Storm, G.; Kiessling, F. Theranostic nanomedicine. *Acc. Chem. Res.* **2011**, *44*, 1029.
(14) Kelkar, S. S.; Reineke, T. M. Theranostics: combining imaging and therapy. *Bioconjugate Chem.* **2011**, *22*, 1879.
(15) Knipe, J. M.; Peters, J. T.; Peppas, N. A. Theranostic agents for intracellular gene delivery with spatiotemporal imaging. *Nano Today* **2013**, *8*, 21−38.
(16) Ryu, J. H.; Koo, H.; Sun, I.-C.; Yuk, S. H.; Choi, K.; Kim, K.; Kwon, I. C. Tumor-targeting multi-functional nanoparticles for theragnosis: new paradigm for cancer therapy. *Adv. Drug Delivery Rev.* **2012**, *64*, 1447−1458.
(17) Shin, S. J.; Beech, J. R.; Kelly, K. A. Targeted nanoparticles in imaging: paving the way for personalized medicine in the battle against cancer. *Integr. Biol.* **2013**, *5*, 29−42.
(18) Svenson, S. Theranostics: are we there yet? *Mol. Pharmacol.* **2013**, *10*, 848−856.
(19) Vivero-Escoto, J. L.; Huxford-Phillips, R. C.; Lin, W. Silica-based nanoprobes for biomedical imaging and theranostic applications. *Chem. Soc. Rev.* **2012**, *41*, 2673−2685.
(20) Wang, H.; Wu, Y.; Zhao, R.; Nie, G. Engineering the assemblies of biomaterial nanocarriers for delivery of multiple theranostic agents with enhanced antitumor efficacy. *Adv. Mater.* **2013**, *25*, 1616−1622.
(21) Choi, K. Y.; Jeon, E. J.; Yoon, H. Y.; Lee, B. S.; Na, J. H.; Min, K. H.; Kim, S. Y.; Myung, S.-J.; Lee, S.; Chen, X. Theranostic nanoparticles based on PEGylated hyaluronic acid for the diagnosis, therapy and monitoring of colon cancer. *Biomaterials* **2012**, *33*, 6186−6193.
(22) Choi, K. Y.; Liu, G.; Lee, S.; Chen, X. Theranostic nanoplatforms for simultaneous cancer imaging and therapy: current approaches and future perspectives. *Nanoscale* **2012**, *4*, 330−342.
(23) Howell, M.; Mallela, J.; Wang, C.; Ravi, S.; Dixit, S.; Garapati, U.; Mohapatra, S. Manganese-loaded lipid-micellar theranostics for simultaneous drug and gene delivery to lungs. *J. Controlled Release* **2013**, *167*, 210−218.
(24) Janib, S. M.; Moses, A. S.; MacKay, J. A. Imaging and drug delivery using theranostic nanoparticles. *Adv. Drug Delivery Rev.* **2010**, *62*, 1052.
(25) Muthu, M. S.; Kulkarni, S. A.; Raju, A.; Feng, S.-S. Theranostic liposomes of TPGS coating for targeted co-delivery of docetaxel and quantum dots. *Biomaterials* **2012**, *33*, 3494−3501.
(26) Xie, J.; Lee, S.; Chen, X. Nanoparticle-based theranostic agents. *Adv. Drug Delivery Rev.* **2010**, *62*, 1064.
(27) Chong, J. Y. T.; Mulet, X.; Waddington, L. J.; Boyd, B. J.; Drummond, C. J. Steric stabilisation of self-assembled cubic lyotropic liquid crystalline nanoparticles: high throughput evaluation of triblock polyethylene oxide-polypropylene oxide-polyethylene oxide copolymers. *Soft Matter* **2011**, *7*, 4768−4777.
(28) Gustafsson, J.; Ljusberg-Wahren, H.; Almgren, M.; Larsson, K. Cubic lipid-water phase dispersed into submicron particles. *Langmuir* **1996**, *12*, 4611−4613.
(29) Larsson, K. Cubic lipid-water phases: structures and biomembrane aspects. *J. Phys. Chem.* **1989**, *93*, 7304−7314.
(30) Monduzzi, M.; Ljusberg-Wahren, H.; Larsson, K. A ^{13}C NMR study of aqueous dispersions of reversed lipid phases. *Langmuir* **2000**, *16*, 7355−7358.
(31) Murgia, S.; Lampis, S.; Zucca, P.; Sanjust, E.; Monduzzi, M. Nucleotide recognition and phosphate linkage hydrolysis at a lipid cubic interface. *J. Am. Chem. Soc.* **2010**, *132*, 16176−16184.
(32) Malmsten, M. Soft drug delivery systems. *Soft Matter* **2006**, *2*, 760.
(33) Borné, J.; Nylander, T.; Khan, A. Effect of lipase on monoolein-based cubic phase dispersion (cubosomes) and vesicles. *J. Phys. Chem. B* **2002**, *106*, 10492−10500.
(34) Caboi, F.; Borné, J.; Nylander, T.; Khan, A.; Svendsen, A.; Patkar, S. Lipase action on a monoolein/sodium oleate aqueous cubic liquid crystalline phase—a NMR and X-ray diffraction study. *Colloids Surf., B* **2002**, *26*, 159−171.
(35) Chessa, M.; Caddeo, C.; Valenti, D.; Manconi, M.; Sinico, C.; Fadda, A. M. Effect of penetration enhancer containing vesicles on the percutaneous delivery of quercetin through new born pig skin. *Pharmaceutics* **2011**, *3*, 497−509.
(36) Gao, X.; Wang, B.; Wei, X.; Men, K.; Zheng, F.; Zhou, Y.; Zheng, Y.; Gou, M.; Huang, M.; Guo, G.; Huang, N.; Qian, Z.; Wei, Y. Anticancer effect and mechanism of polymer micelle-encapsulated quercetin on ovarian cancer. *Nanoscale* **2012**, *4*, 7021−7030.
(37) Han, Q.; Yang, R.; Li, J.; Liang, W.; Zhang, Y.; Dong, M.; Besenbacher, F.; Wang, C. Enhancement of biological activities of nanostructured hydrophobic drug species. *Nanoscale* **2012**, *4*, 2078−2082.
(38) Montalti, M.; Credi, C.; Prodi, L.; Gandolfi, M. T. *Handbook of Photochemistry*; CRC Press: Boca Raton, FL, 2006.
(39) Lakowicz, J. R.; Malicka, J.; D'Auria, S.; Gryczynski, I. Release of the self-quenching of fluorescence near silver metallic surfaces. *Anal. Biochem.* **2003**, *320*, 13.
(40) Rampazzo, E.; Bonacchi, S.; Montalti, M.; Prodi, L.; Zaccheroni, N. Self-organizing core−shell nanostructures: spontaneous accumulation of dye in the core of doped silica nanoparticles. *J. Am. Chem. Soc.* **2007**, *129*, 14251.
(41) Sagalowicz, L.; Michel, M.; Adrian, M.; Frossard, P.; Rouvet, M.; Watzke, H. J.; Yaghmur, A.; De Campo, L.; Glatter, O.; Leser, M. E. Crystallography of dispersed liquid crystalline phases studied by cryo-transmission electron microscopy. *J. Microsc.* **2006**, *221*, 110−121.
(42) Montalti, M.; Prodi, L.; Zaccheroni, N.; Battistini, G.; Marcuz, S.; Mancin, F.; Rampazzo, E.; Tonellato, U. Size effect on the fluorescence properties of dansyl-doped silica nanoparticles. *Langmuir* **2006**, *22*, 5877.
(43) Driever, D. D.; Mulet, X.; Johnston, A. P.; Waddington, J. L.; Thissen, H.; Caruso, F.; Drummond, C. J. Converging layer-by-layer polyelectrolyte microcapsule and cubic lyotropic liquid crystalline

nanoparticle approaches for molecular encapsulation. *Soft Matter* **2011**, *7*, 4257−4266.
(44) Svensson, O.; Thuresson, K.; Arnebrandt, T. Interactions between drug delivery particles and mucin in solution and at interfaces. *Langmuir* **2008**, *24*, 2573−2579.
(45) Guo, C.; Wang, J.; Cao, F.; Lee, R. J.; Zhai, G. Lyotropic liquid crystal systems in drug delivery. *Drug Discovery Today* **2010**, *15*, 1032−1040.
(46) Johnsson, M.; Barauskas, J.; Tiberg, F. Cubic phases and cubic phase dispersions in phospholipid-based systems. *J. Am. Chem. Soc.* **2005**, *127*, 1076−1077.
(47) Spicer, P. T.; Hayden, K. L.; Lynch, M. L.; Ofori-Boateng, A.; Burns, J. L. Novel process for producing cubic liquid crystalline nanoparticles (cubosomes). *Langmuir* **2001**, *17*, 5748−5756.
(48) Angius, R.; Murgia, S.; Berti, D.; Baglioni, P.; Monduzzi, M. Molecular recognition and controlled release in drug delivery systems based on nanostructured lipid surfactants. *J. Phys.: Condens. Matter* **2006**, *18*, S2203.
(49) Clogston, J.; Caffrey, M. Controlling release from the lipidic cubic phase. Amino acids, peptides, proteins and nucleic acids. *J. Controlled Release* **2005**, *107*, 97−111.